Antiferromagnetic Mott insulating state in single crystals of the honeycomb lattice material Na2IrO3

Yogesh Singh, Philipp Gegenwart

Angaben zur Veröffentlichung / Publication details:

Singh, Yogesh, and Philipp Gegenwart. 2010. "Antiferromagnetic Mott insulating state in single crystals of the honeycomb lattice material Na2IrO3." *Physical Review B* 82 (6): 064412. https://doi.org/10.1103/physrevb.82.064412.

Antiferromagnetic Mott insulating state in single crystals of the honeycomb lattice material Na_2IrO_3

Yogesh Singh and P. Gegenwart
I. Physikalisches Institut, Georg-August-Universität Göttingen, D-37077 Göttingen, Germany
(Received 4 March 2010; published 12 August 2010)

We have synthesized single crystals of Na_2IrO_3 and studied their structure, transport, magnetic, and thermal properties using powder x-ray diffraction, electrical resistivity, isothermal magnetization M versus magnetic field H, magnetic susceptibility χ versus temperature T, and heat capacity C versus T measurements. Na_2IrO_3 crystallizes in the monoclinic $C2/c$ (No. 15) type structure which is made up of Na and $NaIr_2O_6$ layers alternately stacked along the c axis. The $\chi(T)$ data show Curie-Weiss behavior at high $T>200$ K with an effective moment $\mu_{\rm eff}=1.82(1)\mu_B$ indicating an effective spin $S_{\rm eff}=1/2$ on the Ir^{4+} moments. A large Weiss temperature $\theta=-116(3)$ K indicates substantial antiferromagnetic interactions between these $S_{\rm eff}=1/2$, Ir^{4+} moments. Anomalies in $\chi(T)$ and $C(T)$ data indicate that Na_2IrO_3 undergoes a transition into a long-range antiferromagnetically ordered state below $T_N=15$ K. The magnetic entropy at T_N is only about 20% of what is expected for $S_{\rm eff}=1/2$ moment ordering. The reduced entropy and the large ratio $\theta/T_N\approx 8$ suggest geometrical magnetic frustration and/or low-dimensional magnetic interactions in Na_2IrO_3. In plane resistivity measurements show insulating behavior. This behavior together with the local-moment magnetism indicates that bulk Na_2IrO_3 is a Mott insulator.

DOI: 10.1103/PhysRevB.82.064412 PACS number(s): 75.40.Cx, 75.50.Lk, 75.10.Jm, 75.40.Gb

I. INTRODUCTION

Layered transition metal oxides provide a playground for various strongly correlated phenomena. The antiferromagnetic Mott insulating ground state in the spin $S=1/2$ square lattice material La_2CuO_4 and the related high-temperature superconductivity in doped materials,[1] spin-triplet superconductivity in Sr_2RuO_4,[2] metamagnetism and quantum criticality in $Sr_3Ru_2O_7$,[3] the metal-insulator transition in $Cd_2Os_2O_7$,[4] and superconductivity in water intercalated Na_xCoO_2,[5] are just some examples of these correlated behaviors.

Electronic correlations are expected to be strongest in $3d$ transition metals and are expected to decrease as one goes to $4d$, and $5d$ transition metals as the extent of the d orbital increases. Thus electronic correlations are expected to be weakest in $5d$ materials and these materials are expected to be metallic due to the larger spatial extent of their d orbitals. However, recently several $5d$ transition metal oxides such as Sr_2IrO_4,[6] $Sr_3Ir_2O_7$,[7] and Ba_2NaOsO_6,[8] have rather surprisingly been discovered to show insulating behaviors. As one goes from $3d$ to $5d$ transition metals the spin-orbit interaction also increases which leads to an effective angular momentum $J_{\rm eff}$ being a good quantum number as opposed to just the spin S. The insulating state in Sr_2IrO_4 has in fact been shown to be a novel Mott-insulating ground state arising from electron correlations among spin-orbit coupled $J_{\rm eff}=1/2$ Ir^{4+} moments.[9,10] Thus in $5d$ systems, the spin-orbit interactions and electron correlations are of comparable strength and an interplay between the two can lead to unusual physics. Recently a new layered iridate Na_2IrO_3 has been studied theoretically and has been suggested to be a $J_{\rm eff}=1/2$ system arising from strong spin-orbit interactions.[11] Correlations between these effective spins has been predicted to lead to an antiferromagnetic insulating state.[11,12] The hexagonal arrangement of the Ir^{4+} moments in Na_2IrO_3 was also suggested to be a realization of the Kane-Mele model which was put forward for quantum spin Hall (QSH) effect in the honeycomb lattice of Graphene.[13,14] Thus Na_2IrO_3 was proposed to be a topological insulator and a possible candidate to show the QSH effect at room temperature.[11] Recently A_2IrO_3 (A=Li, Na) materials have also been suggested[15] to be experimental realizations of the Kitaev model of spins $S=1/2$ sitting on a honeycomb lattice.[16] The model consists of highly frustrated in-plane magnetic interactions which can lead to the spin liquid ground state. In fact, A_2IrO_3 (A=Li, Na) materials had been first suggested in Ref. 10 as possible avenues to explore new physics emerging from the interplay between electronic correlations, spin-orbit physics, and lattice topology. Despite enormous theoretical interest, however, to the best of our knowledge, no experimental information is reported for this material. Herein we report synthesis, structure, electrical transport, magnetic, and thermal properties of single crystalline Na_2IrO_3.

II. EXPERIMENTAL DETAILS

Polycrystalline samples of Na_2IrO_3 and Na_2SnO_3 were synthesized by solid-state synthesis. The starting materials Na_2CO_3 (99.995% Alfa Aesar) and anhydrous IrO_2 ($\geq$99.95% KaiDa) [or Ir metal powder (99.95%, Alfa Aesar) to avoid the possible presence of moisture in starting IrO_2] or SnO_2 (99.995% Alfa Aesar) were mixed in the ratio 1.05:1 and placed in an alumina crucible with a lid and heated to 750 °C in 5 h and held there for 24 h after which it was furnace cooled to room temperature. The resulting mixture was ground and pelletized, placed in an alumina crucible and heated to 900 °C in 6 h and held there for 48 h before cooling to room temperature. The polycrystalline sample of Na_2SnO_3 was reground, pelletized and given a further heat treatment at 1000 °C for 48 h.

To grow single crystals of Na_2IrO_3, the above pellet of Na_2IrO_3 obtained at 900 °C was reground and pelletized and heated to 1050 °C in 5 h, kept at this temperature for 72 h, slowly (10 °C/hr) cooled to 900 °C and then quenched in air. Shiny plate-like single crystals of typical dimensions $1.5\times1.2\times0.1$ mm^3 were found to grow on top of a semi-melted pellet. To optimize the growth, attempts to grow crystals similarly at temperatures between 1000 °C and 1150 °C were attempted. Crystals were not found to grow below about 1000 °C and above about 1100 °C. Thus, $T=1050$ °C seems to be the optimal growth temperature. The structure and composition of the polycrystalline and single crystalline Na_2IrO_3 samples were analyzed using powder x-ray diffraction (XRD) and chemical analysis using energy dispersive x-ray analysis measured with a Philips scanning electron microscope (SEM). The XRD patterns were obtained at room temperature using a Rigaku Geigerflex diffractometer with Cu Kα radiation, in the 2θ range from 10° to 90° with a 0.02° step size. Intensity data were accumulated for 5 s per step. Dc electrical transport was measured on a home built setup using the four probe technique. The isothermal magnetization $M(H)$ and static magnetic susceptibility $\chi(T)$ were measured using a commercial superconducting quantum interference device magnetometer (MPMS5, Quantum Design) and the heat capacity $C(T)$ was measured using a commercial physical property measurement system (PPMS5, Quantum Design).

The magnetic measurements were performed on two kinds of samples. The $M(H)$ and $\chi(T)$ were measured on a collection of randomly oriented crystals with total mass $m=86.34$ mg and the anisotropic $\chi(T)$ data were measured on a collection of six coaligned crystals of total mass $m=8.54$ mg. The heat capacity $C(T)$ was measured on a collection of four crystals of total mass $m=6.83$ mg. The magnetic and thermal properties of the polycrystalline Na_2IrO_3 synthesized at 900 °C were dominated by disorder effects showing a spin-glass like behavior at low temperatures. Therefore, physical properties of only the high quality single crystals are reported in the following as they most likely represent the intrinsic behavior of Na_2IrO_3. The polycrystalline sample, along with the single crystals, is used only for structural characterization.

III. RESULTS

A. Crystal structure and chemical analysis

Powder x-ray diffraction (PXRD) scans of polycrystalline Na_2IrO_3 synthesized at 900 °C are shown in Fig. 2(a). All the lines in the PXRD pattern could be indexed to the monoclinic $C2/c$ (No. 15) structure. Several A_2TO_3 (A=Li, Na, and T=Mn, Ru, Ir, and Pd) type materials are known to adopt a similar structure.[17–20] The structure is made up of layers containing only the A atoms alternating with AT_2O_6 layers stacked along the c axis as shown in Fig. 1(a) for Na_2IrO_3. Within the $NaIr_2O_6$ layers the edge sharing IrO_6 octahedra form a honeycomb lattice as shown in Fig. 1(b). The Na atoms occupy voids between the IrO_6 octahedra. It is known that polycrystalline samples of these materials commonly posses a large amount of disorder arising from faults

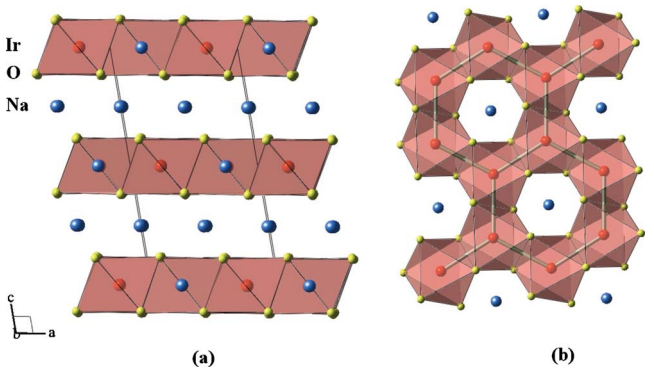

FIG. 1. (Color online) The crystallographic structure of Na_2IrO_3. The Na, Ir, and O atoms are shown as blue (black), red (dark gray), and yellow (light gray) spheres, respectively. (a) The view perpendicular to the c axis showing the layered structure with layers containing only Na atoms alternating slabs of $NaIr_2O_6$ stacked along the c axis. The IrO_6 octahedra are shown in pink with the (red) Ir atoms sitting in the middle. (b) One of the $NaIr_2O_6$ slabs viewed down the c axis to highlight the honeycomb lattice of Ir atoms within the layer. The Na atoms occupy voids between the IrO_6 octahedra.

in the stacking of the AT_2O_6 layers. This leads to anisotropic line shapes in the x-ray diffraction patterns and reduced intensities of peaks between about $2\theta=20°-35°$.[17] To account for the effect of this stacking disorder in Rietveld refinements of the powder x-ray data, site mixing between the A and T sites within the AT_2O_6 layers have been introduced.[17,19,20] We have used a similar approach. Rietveld refinements,[21] shown in Fig. 2(a), of the x-ray pattern gave the unit-cell parameters $a=5.4198(5)$ Å, $b=9.3693(3)$ Å $c=10.7724(7)$ Å, and $\beta=99.568(23)°$ for polycrystalline Na_2IrO_3. The fractional atomic positions, occupancies, isotropic thermal factors, and the reliability parameters R_{wp} and R_p obtained from the Rietveld refinement are given in Table I. We find that a substantial (~15%) site mixing between Ir and Na within the $NaIr_2O_6$ layers is required to fit the x-ray patterns indicating a large amount of atomic or stacking disorder. The introduction of site disorder allows the intensities of peaks between $2\theta=20°-35°$ to be fit quite well, however, the peak profiles are still poorly fit. This leads to large reliability factors as listed in Table I. For a complete structural analysis, stacking faults have to be incorporated in the fits of the x-ray patterns as was done, for example, for Li_2MnO_3.[17]

PXRD scans of crushed single crystals showed large preferred orientation along c axis as expected for a layered material and peaks other than (00l) were much lower in intensity compared to the (00l) lines. However, when plotted on a semi-log plot all the lines in the x-ray patterns could be indexed to the monoclinic $C2/c$ (No. 15) structure. The PXRD data of crushed single crystals is shown in Fig. 2(b) inset along with the peak positions expected for the monoclinic $C2/c$ (No. 15) structure. Due to the large preferred orientation a Rietveld refinement of the PXRD pattern for crushed single crystals was not possible. However, from fitting the peak positions we obtain the lattice parameters $a=5.4262(7)$ Å, $b=9.3858(6)$ Å, $c=10.7688(6)$ Å, and $\beta=99.580(15)°$ for Na_2IrO_3 single crystals. These values are

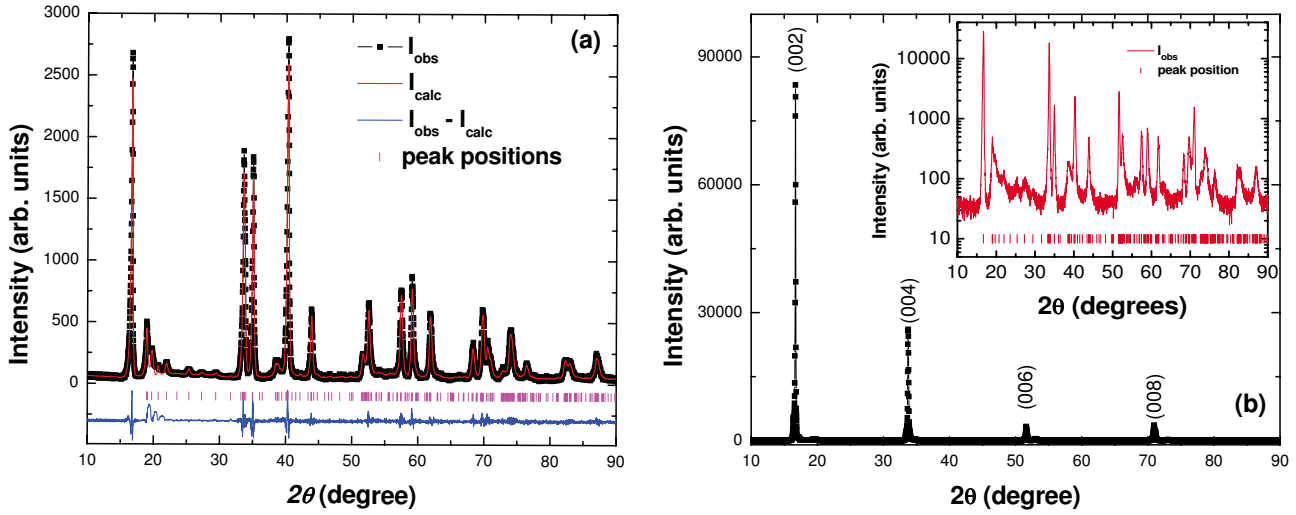

FIG. 2. (Color online) (a) Rietveld refinement of the x-ray diffraction data of polycrystalline Na_2IrO_3 synthesized at 900 °C. The closed symbols represent the observed data, the solid lines represent the fitted pattern, the dotted lines represent the difference between the observed and calculated intensities, and the vertical bars represent the peak positions. (b) X-ray diffraction of c axis oriented single crystals of Na_2IrO_3. The inset shows the powder x-ray diffraction of crushed single crystals on a semi-log plot.

close to those obtained above for the polycrystalline material. The x-ray pattern of surfaces of the as-grown single crystals are shown in Fig. 2(b). Only (00l) reflections expected for the monoclinic $C2/c$ (No. 15) structure are observed indicating that the surface of the crystals are perpendicular to the crystallographic c axis.

An elemental analysis of the single crystals using a SEM showed the presence of only the desired elements Na, Ir, and O in the crystals and an energy dispersive x-ray analysis gave the Na: Ir ratio 1.88:1 which is close to the expected 2:1 ratio for Na_2IrO_3.

B. Electrical resistivity

Figure 3 shows the in-plane dc electrical resistivity of a single crystal of Na_2IrO_3 between $T=80$ and 350 K. The $T=350$ K value $\rho(350\ \mathrm{K}) \approx 21\ \Omega\,\mathrm{cm}$ and the temperature dependence strongly indicate that Na_2IrO_3 is an insulator. Figure 3, inset (a) shows the ρ versus $1/T$ data on a semi-log plot. The data clearly does not follow an Arrhenius law and could not be fit with an activated behavior $\rho(T) \propto exp(-\Delta/T)$ in any extended range of temperature. As shown in Figure 3, inset (b), however, the data follows a $\rho(T) \propto \exp[(\Delta/T)^{1/4}]$ behavior between 100 and 300 K with deviations at higher and lower T. Such a behavior is usually associated with three-dimensional variable-range hopping of carriers localized by disorder. The observation of such a T dependence in Na_2IrO_3 is not understood at present. A similar T dependence was observed for single crystals of Sr_2IrO_4 in a limited T range.[22]

C. Isothermal magnetization

Figure 4 shows a selection of isothermal magnetization M versus magnetic field H data measured at various temperatures T on a collection of randomly oriented crystals with

TABLE I. Structure parameters for Na_2IrO_3 obtained from Rietveld refinements of powder XRD data. The overall isotropic thermal parameter B is defined within the temperature factor of the intensity as $e^{-2B \sin^2\theta/\lambda^2}$.

Atom	x	y	z	Occupancy	B (Å^2)	R_{wp}	R_p
Ir	0.2726(4)	0.0781(3)	0.0005(2)	0.856(3)	0.008(2)	0.212	0.165
Na				0.144(2)	0.013(5)		
Na	0.75	0.25	0.0	0.735(2)	0.009(3)		
Ir				0.265(4)	0.007(1)		
Na	0.50	0.5792(1)	0.25	1.0	0.012(7)		
Na	0.0	0.4720(4)	0.25	1.0	0.009(2)		
Na	0.0	0.75	0.25	1.0	0.016(4)		
O	0.3795(3)	0.2777(4)	−0.1002(1)	1.0	0.013(8)		
O	0.5966(5)	0.0513(3)	0.12128(4)	1.0	0.013(2)		
O	0.6579(4)	0.4130(6)	0.1086(2)	1.0	0.014(6)		

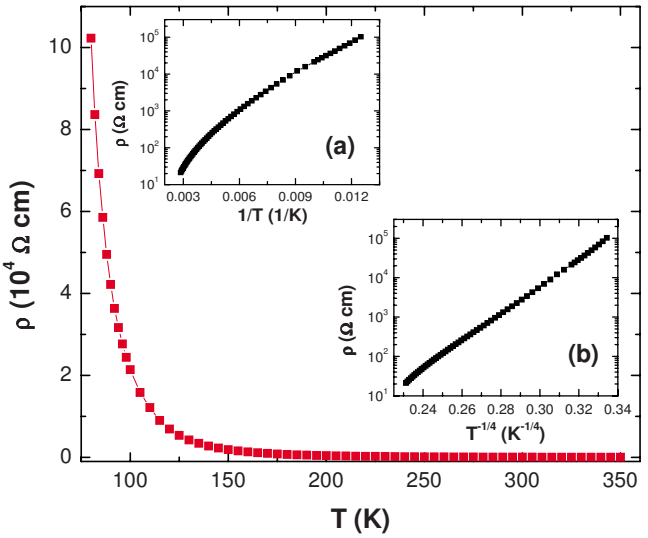

FIG. 3. (Color online) The in-plane electrical resistivity ρ versus temperatures T for a single crystal of Na_2IrO_3. The inset (a) shows the ρ versus $1/T$ data on a semi-log scale. The inset (b) shows the ρ versus $1/T^{1/4}$ data on a semi-log scale.

total mass $m=86.34$ mg. The $M(H)$ data above $T=50$ K are proportional to H indicating the absence of any ferromagnetic impurities in the material. The Fig. 4 inset shows M/H versus H data at $T=100$ K to demonstrate that above ≈ 5000 G, M/H is a constant independent of H. At lower T the $M(H)$ data begin to show curvature indicating the growing influence of magnetic interactions in the material. The $M(H)$ curves for $T=10$ K and $T=1.8$ K lie below the $M(H)$ curve at $T=35$ K due to long-ranged antiferromagnetic ordering at low T in this material as discussed below.

D. Magnetic susceptibility

The inverse magnetic susceptibility $1/\chi_{poly}=H/M$ versus T data between $T=1.8$ and 400 K in an applied magnetic field $H=2$ T for a collection of randomly oriented single crystals of Na_2IrO_3 are shown Fig. 5(a). The $1/\chi_{poly}(T)$ data between $T=200$ and 400 K were fit by the Curie-Weiss (CW) expression $\chi=\chi_0+\frac{C}{T-\theta}$ with χ_0, C, and θ as fitting parameters. The fit, shown in Fig. 5(a) as the solid curve through the data and extrapolated (dashed curve) to $T=0$, gave the values $\chi_0=3.0(7)\times 10^{-5}$ cm^3/mol, $C=0.41(1)$ cm^3 K/mol, and $\theta=-116(3)$ K, respectively. The above value of C corresponds to an effective moment of $\mu_{eff}=1.81(2)$ μ_B assuming a g factor $g=2$. This value of μ_{eff} is close to the value 1.74 μ_B expected for spin$=1/2$ moments. This indicates that the Ir^{4+} moments are in an effective spin $S_{eff}=1/2$ state. The large and negative $\theta=-116(3)$ K further indicates that strong antiferromagnetic interactions exist between these $S_{eff}=1/2$ moments. The deviation of the $1/\chi_{poly}(T)$ data from the Curie-Weiss expression below about $T=100$ K is ascribed to the increasing influence of these antiferromagnetic correlations.

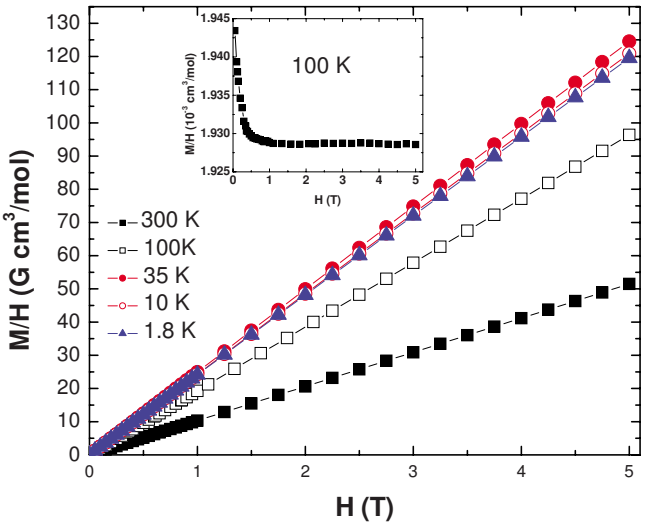

FIG. 4. (Color online) Isothermal magnetization M versus magnetic field H at various temperatures T for a collection of randomly oriented single crystals of Na_2IrO_3. The inset shows the M/H versus H data at $T=100$ T.

The anisotropic magnetic susceptibilities are shown in Fig. 5(b). χ_c and χ_{ab} are the magnetic susceptibilities measured with $H=2$ T applied along the c axis and perpendicular to the c axis, respectively. The susceptibility is weakly anisotropic with the out of plane χ_c being larger than the in-plane χ_{ab} in the whole T range. We find $\frac{\chi_c}{\chi_{ab}}=1.5$ and 2.3 at $T=400$ K and 1.8 K, respectively. The anisotropy can originate from anisotropic Van Vleck paramagnetic susceptibility and/or from anisotropy in the g factor which might both be expected if a trigonal crystal field is present. If we assume $S=1/2$ and fit the $\chi_c(T)$ and $\chi_{ab}(T)$ data to a Curie-Weiss behavior with $\theta=-116$ K obtained above for the χ_{poly} data, we obtain g factors of $g_c=2.68(3)$ and $g_{ab}=1.87(2)$, respectively. Although we have not included an anisotropic Van Vleck term, the above analysis suggests that the g factors might be highly anisotropic. This can be confirmed for example, by electron spin-resonance measurements.

The powder average susceptibility $\chi_{powder}=\frac{\chi_c+2\chi_{ab}}{3}$ and χ_{poly} [from Fig. 5(a)] are also shown in Fig. 5(b). χ_{powder} matches quite well with χ_{poly} except at high T where the small diamagnetic signal from the quartz holder lowers χ_{powder}.

The CW fit obtained in Fig. 5(a) above is also shown as the solid line through the χ_{poly} data in Fig. 5(b). As mentioned before, the data deviate from the CW behavior below about $T=100$ K and pass over a broad maximum at about 23 K before dropping abruptly below $T\approx 15$ K. This can be seen from Fig. 5(b) inset which shows the $\chi_c(T)$ data below $T=40$ K on an expanded scale. The sharp drop below $T_N\approx 15$ K is associated with the onset of long-ranged antiferromagnetic ordering in Na_2IrO_3 while the broad maximum above the ordering is most likely associated with short-ranged order seen commonly in low-dimensional magnetic materials.[1] This is supported by our heat capacity measurements presented below.

E. Heat capacity

Figure 6(a) shows the heat capacity divided by temperature C/T versus temperature T data for single crystals of Na_2IrO_3 measured between $T=2$ and 40 K in a zero applied

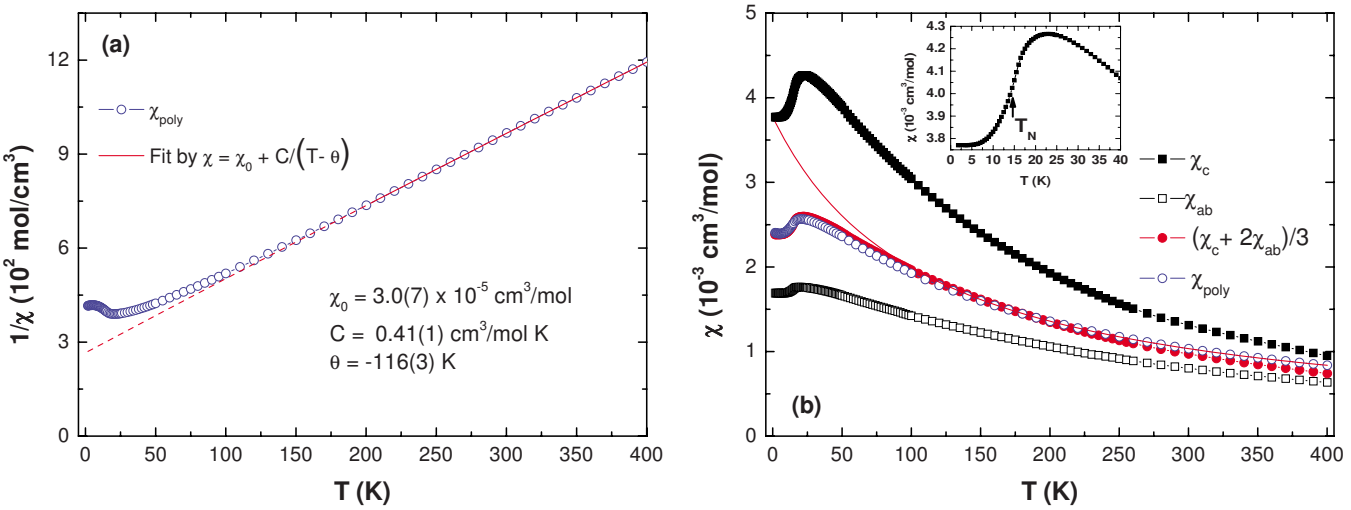

FIG. 5. (Color online) (a) Inverse magnetic susceptibility $1/\chi=H/M$ versus temperature T for a collection of randomly oriented single crystals of Na_2IrO_3 in a magnetic field $H=2$ T. The solid curve through the data is a fit by the expression $\chi=\chi_0+C/(T-\theta)$ and the dashed curve is an extrapolation to $T=0$. (b) The anisotropic magnetic susceptibilities χ_c and χ_{ab} versus T. The powder average susceptibility $(\chi_c+2\chi_{ab})/3$ and the polycrystalline susceptibility χ_{poly} are also shown. The solid curve through the χ_{poly} data is the Curie-Weiss fit. The inset shows the $\chi_c(T)$ data at low T to highlight the broad maximum at $T\approx 23$ K. The arrow indicates the onset temperature $T_N=15$ K for the long-ranged antiferromagnetic ordering.

magnetic field H. The heat capacity of a polycrystalline sample of Na_2SnO_3 is also shown in the same figure as an approximate estimation of the lattice contribution to the heat capacity of Na_2IrO_3. The lambda-like anomaly at $T_N=15$ K for Na_2IrO_3 confirms the bulk nature of the antiferromagnetic ordering observed in the χ data in Fig. 5 above. Figure 6(a) inset shows the C/T versus T data between $T=12$ and 19 K, measured in $H=0$ and $H=7$ T. The slight depression of T_N in an applied magnetic field indicates the antiferromagnetic nature of the ordering.

Figure 6(b) shows the difference heat capacity $\Delta C(T)=C(T)-C_{\text{lattice}}(T)$ and the difference entropy $\Delta S(T)$ obtained by integrating the $\Delta C(T)/T$ versus T data. The ΔC data shows a sharp peak at $T_N=15$ K and a broad tail which extends to higher T. This suggests the presence of short-ranged order above the bulk three-dimensional ordering which occurs at T_N. This is supported by the fact that the entropy just above T_N is $\Delta S(17\ \text{K})\approx 1.2$ J/mol K which is only about 20% of the value $R\ln(2)=5.76$ J/mol K expected for ordering of $S=1/2$ moments. ΔS continues to increase up to the highest T of our measurements.

IV. SUMMARY AND DISCUSSION

Single crystals of Na_2IrO_3 have been grown and their structural, electrical transport, magnetic, and thermal properties investigated. Na_2IrO_3 crystallizes in a layered structure where pure Na layers are stacked alternately with $NaIr_2O_6$

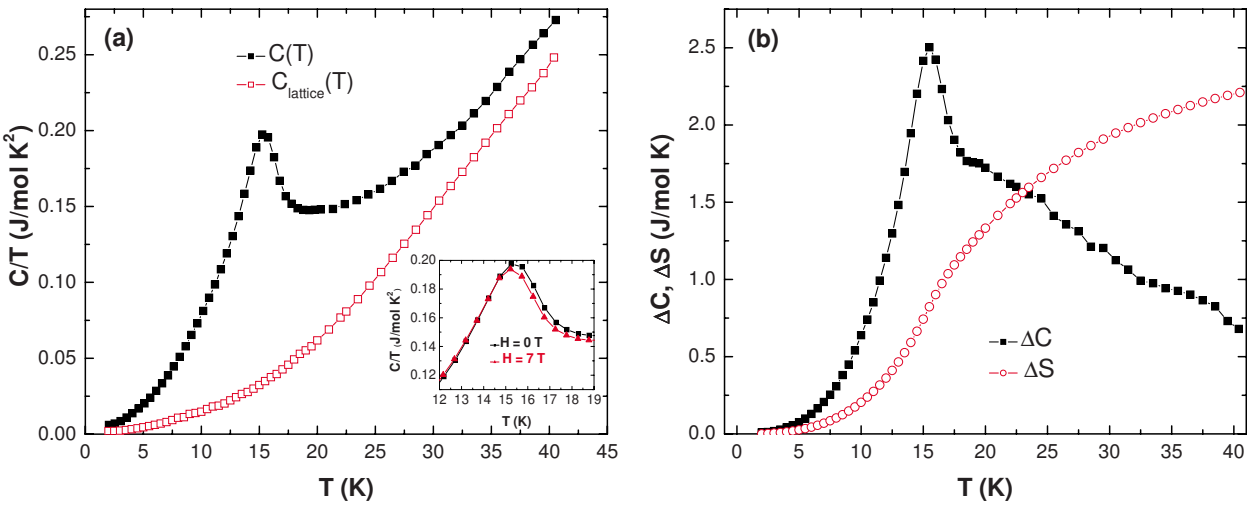

FIG. 6. (Color online) (a) The heat capacity divided by temperature C/T versus T data between $T=1.8$ K and 40 K for single crystals of Na_2IrO_3 and the heat capacity of Na_2SnO_3 as the lattice contribution C_{lattice}/T versus T. The inset shows the C/T versus T data in $H=0$ and 7 T applied magnetic field. (b) The difference heat capacity ΔC and difference entropy ΔS versus T data between $T=1.8$ and 40 K.

slabs along the *c* axis of the monoclinic unit cell. Within the $NaIr_2O_6$ layers, the Ir^{4+} moments sit on a honeycomb lattice. Electrical transport within the *ab* plane shows insulating behavior. Magnetic susceptibility measurements provide evidence that the Ir atoms carry effective $S_{\text{eff}}=1/2$ moments and they have strong antiferromagnetic interactions as evidenced by a large and negative Weiss temperature $\theta=-116(3)$ K. The magnetic susceptibility is slightly anisotropic with $\chi_c > \chi_{ab}$ for all measured *T*.

The $\chi(T)$ deviates from Curie-Weiss behavior below $T \sim 100$ K and passes over a broad maximum around $T=23$ K before decreasing strongly below the three-dimensional antiferromagnetic ordering temperature $T_N=15$ K. At the lowest $T=1.8$ K, $\chi(T)$ saturates to a large and finite value. This indicates that the magnetic ordering is most likely noncollinear. It is difficult to decide the ordering direction from our measurements. The reduction in the absolute value of χ below T_N is larger for χ_c but the change in slope at T_N is stronger for χ_{ab}.

A much smaller $T_N=15$ K compared to the Weiss temperature $\theta=-116(3)$ K indicates frustrated magnetic interactions in Na_2IrO_3. This is consistent with a recent theoretical study which has made estimates of the ratio between the nearest-neighbor (NN) and next-nearest-neighbor (NNN) magnetic interactions and find that $\frac{J_{\text{NNN}}}{J_{\text{NN}}}=0.47$, indicating strongly frustrated magnetic interactions.[12] The maximum in $\chi(T)$ above the long-ranged ordering temperature T_N is commonly observed in low-dimensional materials where short-ranged magnetic order develops (within the $NaIr_2O_6$ layers in Na_2IrO_3 for example) well above T_N and long-ranged magnetic order only occurs when the interplanar interactions become important. The presence of short-ranged magnetic order is also supported by our heat capacity measurements. The $C(T)$ shows a sharp lambda-like anomaly at $T_N=15$ K indicating bulk magnetic ordering. However, the difference heat capacity $\Delta C(T)$ shows a broad tail extending to much higher *T* above T_N and the difference entropy ΔS just above T_N is only about 20% of what is expected for ordering of spin $S=1/2$ moments. The $\Delta S(T)$ also continues to increase upto the highest *T* of our measurements. An incorrect estimation of the lattice contribution to $C(T)$ can lead to a reduced $\Delta S(T)$. However, if we estimate the entropy by integrating the total $C(T)/T$ versus *T* data without any lattice subtraction, we still end up with only $\approx 30\% R \ln(2)$ at T_N suggesting that the reduced entropy is intrinsic to Na_2IrO_3 and most likely occurs due to the development of short-ranged magnetic order above T_N.

There has been a lot of recent theoretical interest in Na_2IrO_3 with suggestions of a topological band insulator[11] or a magnetically ordered Mott insulator[12] being possible ground states for this system. Our electrical transport results indicate insulating behavior consistent with the above predictions. However, our magnetic measurements indicate local-moment magnetism and long-range antiferromagnetic ordering which is not consistent with the topological band insulator picture above.

Further experiments will be needed to investigate the importance of spin-orbit interactions and the strength of electronic correlations in Na_2IrO_3 as has been suggested in previous theoretical work.[10–12] The magnetic structure and the nature of the magnetic interactions will also need further work to compare with the various proposed magnetic ground states[15] although the spin-liquid phase near the Kitaev limit seems unlikely from our results.[15]

To summarize, single crystals of Na_2IrO_3 have been synthesized. From magnetic, thermal, and transport measurements we conclude that Na_2IrO_3 is a quasi-low-dimensional, magnetically frustrated material which undergoes long-ranged antiferromagnetic ordering below $T_N=15$ K into most likely a noncollinear magnetic structure. The insulating in-plane electrical transport together with the local-moment magnetism indicate that Na_2IrO_3 is a Mott insulator.

ACKNOWLEDGMENTS

Y.S. acknowledges correspondence and discussion with G. Khaliullin. Y.S. would like to thank the Alexander von Humboldt foundation for support.

[1] For a review, see D. C. Johnston, in *Handbook of Magnetic Materials*, edited by K. H. J. Buschow (Elsevier, Amsterdam, 1997), Vol. 10, Chap. 1, pp. 1–237.
[2] K. D. Nelson, Z. Q. Mao, Y. Maeno, and Y. Liu, Science **306**, 1151 (2004).
[3] R. A. Borzi, S. A. Grigera, J. Farrell, R. S. Perry, S. J. S. Lister, S. L. Lee, D. A. Tennant, Y. Maeno, and A. P. Mackenzie, Science **315**, 214 (2007).
[4] D. Mandrus, J. R. Thompson, R. Gaal, L. Forro, J. C. Bryan, B. C. Chakoumakos, L. M. Woods, B. C. Sales, R. S. Fishman, and V. Keppens, Phys. Rev. B **63**, 195104 (2001).
[5] K. Takada, H. Sakurai, E. Takayama-Muromachi, F. Izumi, R. A. Dilanian, and T. Sasaki, Nature (London) **422**, 53 (2003).
[6] M. K. Crawford, M. A. Subramanian, R. L. Harlow, J. A. Fernandez-Baca, Z. R. Wang, and D. C. Johnston, Phys. Rev. B **49**, 9198 (1994).
[7] G. Cao, Y. Xin, C. S. Alexander, J. E. Crow, P. Schlottmann, M. K. Crawford, R. L. Harlow, and W. Marshall, Phys. Rev. B **66**, 214412 (2002).
[8] A. S. Erickson, S. Misra, G. J. Miller, R. R. Gupta, Z. Schlesinger, W. A. Harrison, J. M. Kim, and I. R. Fisher, Phys. Rev. Lett. **99**, 016404 (2007).
[9] B. J. Kim, H. Jin, S. J. Moon, J.-Y. Kim, B.-G. Park, C. S. Leem, Yu. Jaejun, T. W. Noh, C. Kim, S.-J. Oh, J.-H. Park, V. Durairaj, G. Cao, and E. Rotenberg, Phys. Rev. Lett. **101**, 076402 (2008).
[10] G. Jackeli and G. Khaliullin, Phys. Rev. Lett. **102**, 017205 (2009).
[11] A. Shitade, H. Katsura, J. Kunes, X.-L. Qi, S.-C. Zhang, and N. Nagaosa, Phys. Rev. Lett. **102**, 256403 (2009).
[12] H. Jin, H. Kim, H. Jeong, C. Kim, and J. Yu, arXiv:0907.0743 (unpublished).
[13] C. L. Kane and E. J. Mele, Phys. Rev. Lett. **95**, 146802 (2005).

[14] C. L. Kane and E. J. Mele, Phys. Rev. Lett. **95**, 226801 (2005).
[15] J. Chaloupka, G. Jackeli, and G. Khaliullin, Phys. Rev. Lett. **105**, 027204 (2010).
[16] A. Kitaev, Ann. Phys. (N.Y.) **321**, 2 (2006).
[17] J. Breger, M. Jiang, N. Dupre, Y. S. Meng, Y. Shao-Horn, G. Ceder, and C. P. Grey, J. Solid State Chem. **178**, 2575 (2005).
[18] H. Kobayashi, R. Kanno, Y. Kawamoto, M. Tabuchi, O. Nakamura, and M. Takano, Solid State Ionics **82**, 25 (1995).
[19] H. Kobayashi, M. Tabuchi, M. Shikano, H. Kageyama, and R. Kanno, J. Mater. Chem. **13**, 957 (2003).
[20] R. V. Panina, N. R. Khasanova, A. M. Abakumov, Evgeny V. Antipov, G. V. Tendeloo, and W. Schnelle, J. Solid State Chem. **180**, 1566 (2007).
[21] A. C. Larson and R. B. Von Dreele, Los Alamos National Laboratory Report No. LAUR 86–748, 2000 (unpublished); B. H. Toby, J. Appl. Crystallogr. **34**, 210 (2001).
[22] G. Cao, J. Bolivar, S. McCall, J. E. Crow, and R. P. Guertin, Phys. Rev. B **57**, R11039 (1998).